chemistry

MDPI

Article

Lactone-Terminated Self-Assembled Monolayers for Mimicking Nanoscale Polyester Surfaces

Pooria Tajalli [1], Jennifer M. Hernandez Rivera [1], Mina Omidiyan [1], Jong Moon Lee [1], Hung-Vu Tran [1,2] and T. Randall Lee [1,*]

[1] Department of Chemistry and the Texas Center for Superconductivity, University of Houston, 4800 Calhoun Road, Houston, TX 77204-5003, USA
[2] NTT Hi-Tech Institute, Nguyen Tat Thanh University, 298-300A Nguyen Tat Thanh Street, District 4, Ho Chi Minh City 7280, Vietnam
* Correspondence: trlee@uh.edu

Abstract: Two series of lactone-terminated alkanethiol adsorbates with five- and six-membered lactone groups, **γ-COCnSH** and **δ-COCnSH** (n = 11, 12), were synthesized and employed to create nanoscale self-assembled monolayers (SAMs) on gold substrates to mimic the properties of commercially available poly(lactic-co-glycolic acid) (PLGA) and poly(glycolic acid) (PGA) surfaces. ^{1}H and ^{13}C nuclear magnetic resonance (NMR) were employed to characterize the adsorbate molecules. The thicknesses of the corresponding self-assembled monolayers (SAMs) were evaluated by ellipsometry. The conformational characteristics of the SAMs were analyzed using polarization modulation infrared reflection adsorption spectroscopy (PM-IRRAS), with a focus on the C-H antisymmetric stretching vibrations of the alkyl spacers. To evaluate the packing densities of the monolayers, X-ray photoelectron spectroscopy (XPS) measurements were performed. Separately, contact angle measurements provided insights into the wettability of the surfaces. Remarkably, the contact angle data across a broad range of probe liquids for the **γ-COC11SH** and **γ-COC12SH** SAMs were consistently similar to each other and to the contact angle values of the PLGA surface, rather than to PGA. This finding suggests that the lactone-terminated SAMs investigated in this study effectively mimic nanoscale polyester surfaces, enabling the exploration of interfacial properties of polyesters in the absence of swelling and/or surface reconstruction phenomena.

Keywords: lactone-terminated; self-assembled monolayers (SAMs); polymer mimics; polyesters; poly(lactic-co-glycolic acid) (PLGA); poly(glycolic acid) (PGA); wettability; interfacial properties

Citation: Tajalli, P.; Hernandez Rivera, J.M.; Omidiyan, M.; Lee, J.M.; Tran, H.-V.; Lee, T.R. Lactone-Terminated Self-Assembled Monolayers for Mimicking Nanoscale Polyester Surfaces. *Chemistry* **2024**, *6*, 666–676. https://doi.org/10.3390/chemistry6040039

Academic Editors: Valentine Vullev and Igor Alabugin

Received: 30 May 2024
Revised: 25 July 2024
Accepted: 25 July 2024
Published: 31 July 2024

1. Introduction

In 1833, Joseph-Louis Gay-Lussac pioneered the synthesis of polyesters from lactic acid [1]. Since then, various types of biodegradable polyesters, such as poly(glycolic acid) (PGA), poly(lactic acid) (PLA), and poly(lactic-co-glycolic acid) (PLGA), have been successfully synthesized [2,3]. These polyesters have attracted considerable attention due to their ability to undergo degradation under in vivo conditions, rendering them suitable for applications in surgical operations and regenerative medicine [2,3]. Among these polyesters, PLA has emerged as one of the most widely used biopolymers, renowned for its high rigidity and ability to degrade within a span of months [2]. On other hand, PGA stands out as a crystalline polymer that undergoes more rapid degradation in natural environments when compared to other polyesters. Consequently, blending PLA and PGA in various ratios enables the generation of PLGA with distinct molecular weights, crystallinity levels, mechanical properties, and rates of biodegradability [4].

Polyester polymers exhibit two distinct morphologies: amorphous and crystalline. In the amorphous state, the polymer chains adopt irregular coiling configurations, whereas in the crystalline state, the polymer chains align parallel to each other [2]. Despite their

inherent stability, biodegradable polyester polymers are prone to swelling when exposed to water [5]. Polymer swelling occurs when water molecules diffuse into the polymer matrix, allowing the polymer chains to undergo structural reorganization into their most favorable conformation, often giving rise to the development of a crystalline structure [6–8]. As a consequence, the swelling of polymers induced by water can significantly alter the hydrophobic nature of the polymer layers, posing challenges in the study of interfacial properties of these layers when in contact with water [9].

Organic thin films such as self-assembled monolayers (SAMs) have gained widespread use as a means of modifying the interfacial properties of various surfaces. These thin-film coatings have been employed in a range of applications, including polycarbonate mimics [10], microelectromechanical system (MEMs) lubricants [11], hydrogenation reaction catalysts [12,13], metal surface anti-corrosion agents [14,15], and anti-adhesive films for surfaces and biosensors [16,17]. The popularity of SAMs stems from their easy production and manipulation. This study is part of a series of projects focused on the synthesis and characterization of self-assembled monolayers designed to mimic polymeric surfaces [10,18,19]. In this study, we designed, fabricated, and studied monolayer films that closely resemble the surfaces of widely used polyesters. Specifically, we prepared SAMs on gold surfaces by adsorbing alkanethiols terminated with lactone moieties. These SAMs serve as mimics for commercially available PGA and PLGA. Our investigation centers on SAMs derived from **γ-COCnSH** (n = 11 and 12) and **δ-COCnSH** (n = 11 and 12), which possess terminal lactone groups (see Figure 1). We propose that SAMs derived from **γ-COCnSH** and **δ-COCnSH** will expose interfaces consisting of lactone groups capable of emulating the surfaces of PGA and PLGA; such films will resist surface reconstruction or swelling typically observed in bulk polymer coatings. Consequently, we synthesized two distinct sets of adsorbates with varying ring sizes of lactone groups for generating unique lactone-terminated SAMs that exhibit structural similarity to the backbones of PGA and PLGA.

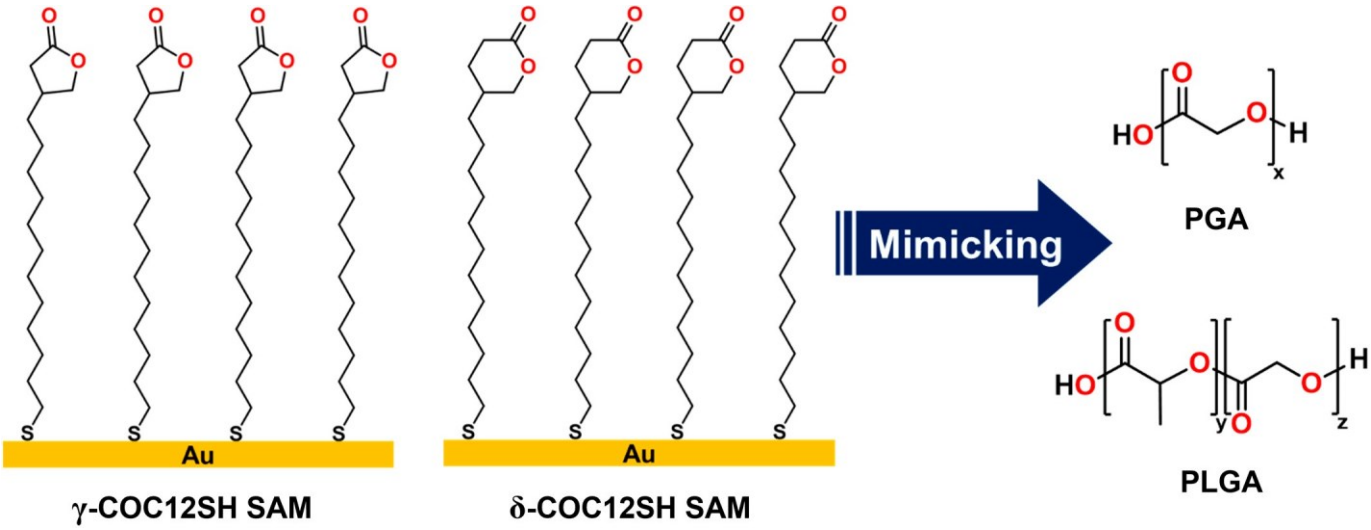

Figure 1. Molecular structures of the SAMs and polyesters examined in this study.

2. Materials and Methods

2.1. Materials

Polyglycolic acid (PGA) sutures and polyglactin 910 (PLGA) sutures were purchased from HexaDental (Commerce, CA, USA) and Ethicon Inc. (Raritan, NJ, USA), respectively. The following chemicals and materials were obtained from Sigma-Aldrich (St. Louis, MO, USA): 1,12-dibromododecane, dimethyl malonate, ethyl bromoacetate, methyl 3-bromopropionate, potassium thioacetate (KSAc), sodium hydride (NaH, 60% dispersion in mineral oil), lithium chloride (LiCl), iodine, triethylamine, lithium aluminum hydride (LAH), barium manganate ($BaMnO_4$), manganese dioxide (MnO_2), hexafluoroisopropanol,

dimethyl sulfoxide (DMSO), acetyl chloride, tetrahydrofuran (THF), dichloromethane (DCM), formamide (FA), *N*-methylformamide (MF), glycerol (Gly), acetonitrile (MeCN), *N*,*N*-dimethylformamide (DMF), decalin (DC), hexadecane (HD), squalane (SQ), and diiodomethane (DIM), which were used without further purification. 2,2′-Azobis (2-methylpropionitrile) (AIBN) was purchased from Sigma-Aldrich and recrystallized in methanol (Oakwood) before use. Undec-10-enyl bromide, magnesium sulfate ($MgSO_4$), dithiothreitol (DTT), sodium bicarbonate ($NaHCO_3$), and diethyl ether (Et_2O) were purchased from Oakwood and used without further purification. Ethanol (Fisher, Portsmouth, NH, USA), ethyl acetate (Fisher), hydrochloric acid (HCl) (Thomas Scientific, Swedesboro, NJ, USA), *n*-hexanes (VWR), and thioacetic acid (TCI) were used as received. Chromium rods (99.9%) were obtained from R. D. Mathis, and gold shot (99.999%) was purchased from Kamis Incorporated (Croton Falls, NY, USA). Test-grade polished single-crystal silicon(100) wafers were acquired from University Wafer and cleaned by rinsing with absolute ethanol from Aaper Alcohol and Chemical Co. (Shelbyville, KY, USA) before use.

2.2. Preparation of the SAMs

Au substrates were fabricated by evaporating gold onto Si(100) wafers using thermal evaporation under vacuum conditions (pressure less than 6×10^{-5} torr). Initially, a 100 Å thin layer of Cr was deposited to enhance adhesion, followed by the deposition of 1000 Å of Au at a rate of 1 Å/s. After deposition, the substrates were rinsed with ethanol and dried using ultra-pure nitrogen gas. Multiple 1 mM aliquots of the adsorbate solution in ethanol were prepared in 40 mL vials. Two sections of cut Au slides were immersed in the adsorbate solution and incubated in the dark at room temperature for 24 h. Following incubation, all films were rinsed with THF and absolute ethanol and subsequently dried using ultra-pure nitrogen gas.

2.3. Characterization of the SAMs

Thickness measurements were performed using an Alpha-SE J.A. Woollam Co. (Lincoln, NE, USA) Spectroscopic Ellipsometer, which was equipped with a multi-wavelength LED laser operating in the range of 400 to 800 nm. The measurements were conducted at an incident angle of 70°. Optical constants were obtained for each film, serving as a reference for determining the thickness values. The reported thickness values represent an average of six measurements, with three measurements taken per slide.

X-ray photoelectron spectroscopy (XPS) measurements were conducted using a PHI 5700 X-ray photoelectron spectrometer (Chanhassen, MN, USA). The instrument was equipped with a monochromatic A1 Kα X-ray source with an energy of 1486.7 eV, which was incident at a 90° angle relative to the axis of the hemispherical energy analyzer. The takeoff angle was set at 45°, and a pass energy of 23.5 eV was used. To establish a reference, the binding energy of the Au 4f7/2 peak was set at 84.0 eV for each spectrum.

Polarization modulation infrared reflection adsorption spectroscopy (PM-IRRAS) spectra were acquired using a Nicolet Nexus 670 Fourier transform spectrometer (Waltham, MA, USA). The instrument was equipped with a mercury-cadmium-telluride (MCT) detector (Waltham, MA, USA) and a Hinds Instrument PEM-90 photoelastic modulator (Hillsboro, OR, USA). The measurements were performed at an incident angle of 80° relative to the surface normal, using p-polarized light.

Contact angle data were obtained using a compact high-resolution CMOS camera (DCC1645C, San Jose, CA, USA) coupled with a 12× zoom lens (MVL12X12Z). A Matrix Technologies micro-Electrapette 25 (Menlo Park, CA, USA) was utilized to dispense liquids from a disposable pipette tip. The liquids were dispensed at a rate of 1 μL/s to measure the advancing contact angle (θa), and subsequently withdrawn at the same speed to measure the receding contact angle (θr). Each contact angle data point represents an average of three measurements, with three measurements taken per slide.

2.4. Spin-Coating Method

The polyglycolic acid and polyglactin 910 were dissolved in hexafluoroisopropanol at 65 °C at a concentration of 2 wt%. Subsequently, 0.5 mL of the sample was carefully dropped onto a glass surface and the substrate was spun at 2000 rpm for 1 min to achieve uniform coating. The polymer films were then dried in an oven at 60 °C for 6 h.

2.5. Synthesis Procedure

The synthesis procedures used in this study are detailed in the Supporting Information, which are presented graphically as Schemes S1–S4 and in Figures S1–S19.

3. Results and Discussion

3.1. Ellipsometric Measurements of the SAMs

The monolayer films were characterized using ellipsometry after immersing gold slides in ethanolic solutions of the adsorbates for a duration of 24 h [20]. The ellipsometry data are presented in Table 1. To provide a reference for our newly studied SAMs, the thicknesses of SAMs formed by well-established *n*-alkanethiols having similar chain lengths are also included in Table 1, Row 1 [19]. The accuracy of the ellipsometric measurements is subject to an uncertainty of ±2 Å. It is worth noting that the thickness of our reference SAMs derived from **C18SH** falls within the experimental error range of the values reported in the literature [19,21]. However, it is important to acknowledge that these reported thickness values can vary depending on the quality and cleanliness of the gold substrates.

Table 1. Ellipsometric thicknesses of SAMs derived from **C18SH** and the lactone thiols.

Adsorbate	Thickness (Å)
C18SH	20 ± 1
γ-COC11SH	15 ± 1
γ-COC12SH	16 ± 1
δ-COC11SH	16 ± 1
δ-COC12SH	17 ± 1

A comparison between lactone-terminated monolayers and their corresponding *n*-alkanethiols SAMs having similar alkyl chain lengths revealed differences in their thicknesses. The **γ-COCnSH** and **δ-COCnSH** monolayers were found to be thinner compared to the analogous *n*-alkanethiols SAMs. This observation can be attributed to the presence of the bulky lactone rings on the **γ-COCnSH** and **δ-COCnSH** adsorbate molecules, which can plausibly lead to a decrease in molecular packing density on the gold surface. It is worth noting that the thicknesses of the **γ-COC11SH** SAMs (15 Å) and **γ-COC12SH** SAMs (16 Å) fall within the experimental error range of the thickness measured for the **δ-COC11SH** SAMs (16 Å) and **δ-COC12SH** SAMs (17 Å). This consistency in thickness supports the findings from the polarization modulation infrared reflection adsorption spectroscopy (PM-IRRAS) data obtained for the films (vide infra).

3.2. XPS Analysis of the SAMs

X-ray photoelectron spectroscopy (XPS) is a surface-sensitive analytical technique widely used for the quantitative determination of the elemental surface composition [22,23]. By detecting the binding energy (BE) of emitted photoelectrons from individual atoms, XPS provides distinctive sets of characteristic peaks that enable the determination of the chemical environment and oxidation state of the atoms [22,23]. In this study, XPS was employed to examine the S 2p, C 1s, and O 1s regions of the investigated monolayers. The XPS spectra, shown in Figure 2, were referenced to the Au 4f7/2 peak at 84 eV, enabling accurate comparisons and analysis of the observed peaks and their chemical properties.

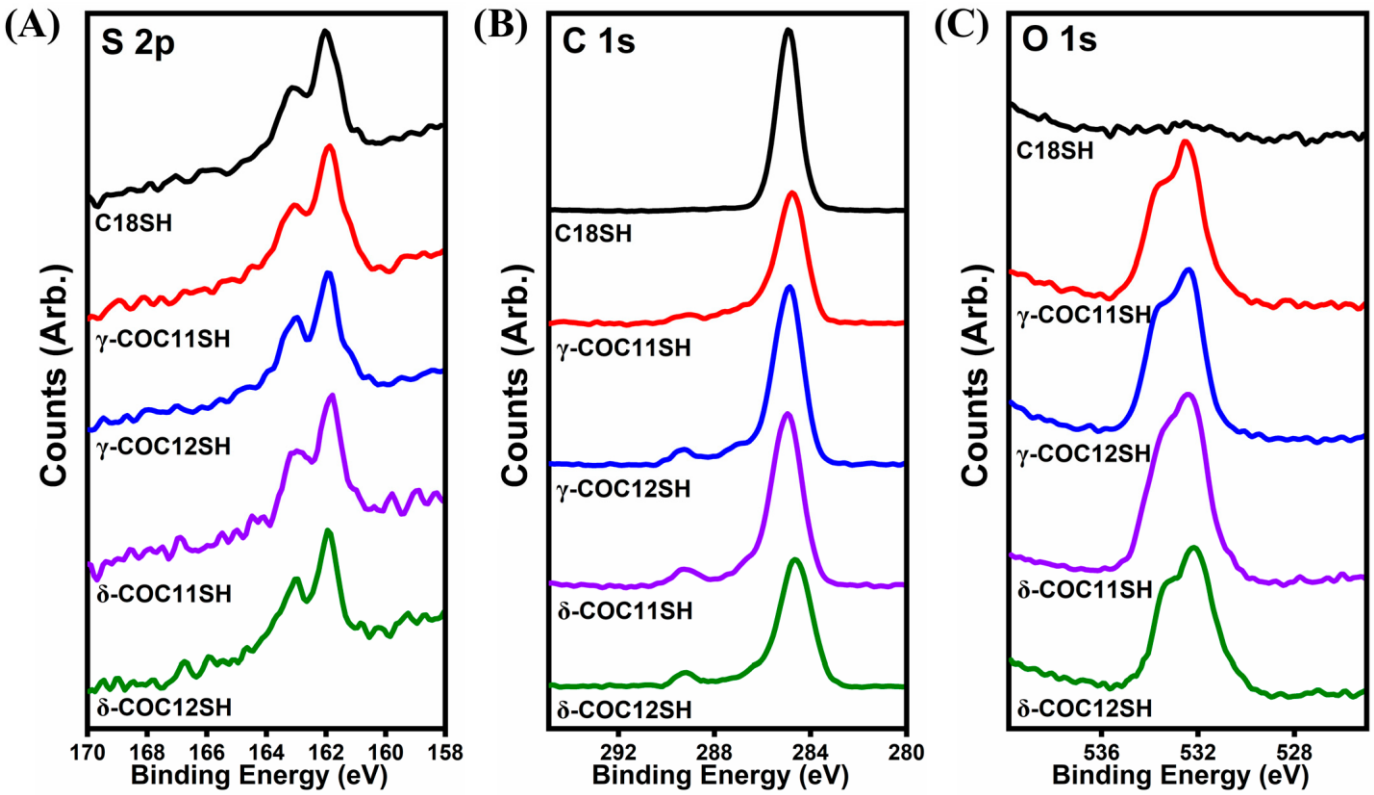

Figure 2. XPS spectra for the (**A**) S 2p, (**B**) C 1s, and (**C**) O 1s of the **C18SH**, **γ-COC11SH**, **γ-COC12SH**, **δ-COC11SH**, and **δ-COC12SH** SAMs.

The XPS analyses revealed distinct features in the spectra of the investigated monolayers. Figure 2A displays a spin-orbit-split doublet for bound thiol, with peaks observed at ~162 and ~163.2 eV, in a 2:1 ratio, assigned to S 2p3/2 and S 2p1/2, respectively [19]. Conversely, unbound thiol groups and highly oxidized sulfur species are known to exhibit spin-orbit-split S 2p peaks centered at ~163.3 and ~167.6 eV, respectively. Notably, the absence of both ~163.3 and ~167.6 eV peaks in Figure 2A is consistent with the absence of significant unbound or oxidized sulfur species in the SAMs derived from *n*-alkanethiols and lactone-terminated thiols evaluated in this study [19,23]. In the C 1s region, the peak position for the CH_3/CH_2 unit in **C18SH**, **γ-COC11SH**, **γ-COC12SH**, **δ-COC11SH**, and **δ-COC12SH** SAMs were observed at ~284.8 eV (Figure 2B). Additionally, the XPS spectra revealed two additional peaks for **γ-COC11SH**, **γ-COC12SH**, **δ-COC11SH**, and **δ-COC12SH**, with binding energies (BEs) of ~286.8 eV for C–O species and ~289.3 eV for C=O species. These findings are consistent with the presence of lactone groups within the monolayers [24,25]. Furthermore, Figure 2C shows the peak positions in the O 1s region, with BEs of ~532.4 eV for C=O species and ~533.8 eV for C–O species, corroborating the presence of these functional groups within the monolayers [24,25].

The relative packing density of the SAMs was assessed by calculating the ratio of integrated areas of peaks in the S 2p region to the integrated area of peaks in the Au 4f region. To normalize this ratio, the S/Au ratio was set to 100% for the **C18SH** SAMs as a reference [19]. Table 2 presents the binding energies (BEs) of the S 2p3/2 and C 1s bands for all five SAMs, which are found to be within experimental error. All four SAMs consisting of **γ-COC11SH**, **γ-COC12SH**, **δ-COC11SH**, and **δ-COC12SH** exhibit high packing densities of 91%, 90%, 87%, and 85%, respectively. Notably, the packing density of the **γ-COC11SH** and **γ-COC12SH** SAMs was reproducibly greater than that of the **δ-COC11SH** and **δ-COC12SH** SAMs. This unremarkable difference in packing density (assuming the difference is real) could be attributed to the size disparity between the lactone rings present in the respective SAMs. The smaller lactone rings in the **γ-COC11SH**

and **γ-COC12SH** SAMs would enable a more efficient packing arrangement, leading to a denser SAM structure. In contrast, the larger and bulkier lactone rings in the **δ-COC11SH** and **δ-COC12SH** SAMs might reflect increased steric hindrance and thereby limit the degree of packing, leading to a lower packing density. On the whole, the C 1s binding energies are consistent with a model in which all of the lactone-terminated SAMs are densely packed, given that their C 1s binding energies are indistinguishable from those of the densely-packed SAMs derived from **C18SH** [26]. It is worth noting that densely packed films act as superior insulators compared to loosely packed films, effectively preventing the discharge of positive charges generated by photoelectron emission and resulting in higher C 1s binding energies [26].

Table 2. Binding energies and relative packing densities of the SAMs derived from **C18SH**, **γ-COC11SH**, **γ-COC12SH**, **δ-COC11SH**, and **δ-COC12SH**.

Adsorbate	S $2p_{3/2}$ (eV)	C 1s (CH_2) (eV)	C 1s (C–O) (eV)	C 1s (C=O) (eV)	O 1s (C–O) (eV)	O 1s (C=O) (eV)	Relative Packing Density (%)
C18SH	162	284.9	–	–	–	–	100
γ-COC11SH	161.9	284.8	286.8	289.2	533.3	532.5	91 ± 4
γ-COC12SH	161.9	284.9	286.9	289.3	533.3	532.4	90 ± 2
δ-COC11SH	161.9	284.9	286.8	289.3	533.2	532.5	87 ± 2
δ-COC12SH	161.9	284.7	286.6	289.2	533.2	532.3	85 ± 3

3.3. PM-IRRAS Analysis of the SAMs

Polarization modulation infrared reflection adsorption spectroscopy (PM-IRRAS) was employed to investigate the structural characteristics of SAMs, including chain orientation and conformational order [27]. Specifically, the degree of conformational order, or "crystallinity", of the alkyl chains was assessed by analyzing the peak position of the antisymmetric methylene C–H stretching vibration (υ_{as}^{CH2}) [27]. In highly crystalline films, this band is observed at approximately ~2918 cm^{-1}, indicating well-ordered alkyl chains that are predominantly trans-extended. However, the presence of gauche defects in the alkyl chains causes a blue-shift of this band to higher wavenumbers [28,29]. Figure 3 illustrates the PM-IRRAS spectra of the C–H stretching region for the SAMs generated from **C18SH** and the lactone-terminated monolayers, and Table 3 provides a tabulated summary of the corresponding spectral data.

Table 3 presents the peak positions and assignments of the C–H stretching region for the investigated SAMs. The **γ-COC11SH** and **γ-COC12SH** SAMs exhibit a υ_{as}^{CH2} band at ~2920 cm^{-1}, indicating a well-ordered monolayer with predominantly trans-extended alkyl chains. The proximity of this peak position to the υ_{as}^{CH2} band observed in trans-extended alkyl chains of **C18SH** (~2918 cm^{-1}) generally supports this interpretation [28,29]. In contrast, the **δ-COC11SH** and **δ-COC12SH** SAMs exhibit a υ_{as}^{CH2} band at ~2923 cm^{-1}, indicating a lower degree of conformational order compared to the **γ-COC11SH** and **γ-COC12SH** SAMs. Notably, the monolayers containing five-membered lactone rings, as studied here, exhibit a similar conformational order to our previous study involving carbonate-terminated films with a 12-carbon chain length [10]. This observation aligns with the findings obtained from ellipsometric thickness measurements and XPS discussed earlier (vide supra). It is plausible that the enhanced conformational order observed in the γ-lactone-terminated SAMs arises from the smaller terminal five-membered ring lactone groups compared to the larger terminal six-membered ring lactone groups in the δ-lactone-terminated films, where the latter bulkier tail groups inhibit dense packing.

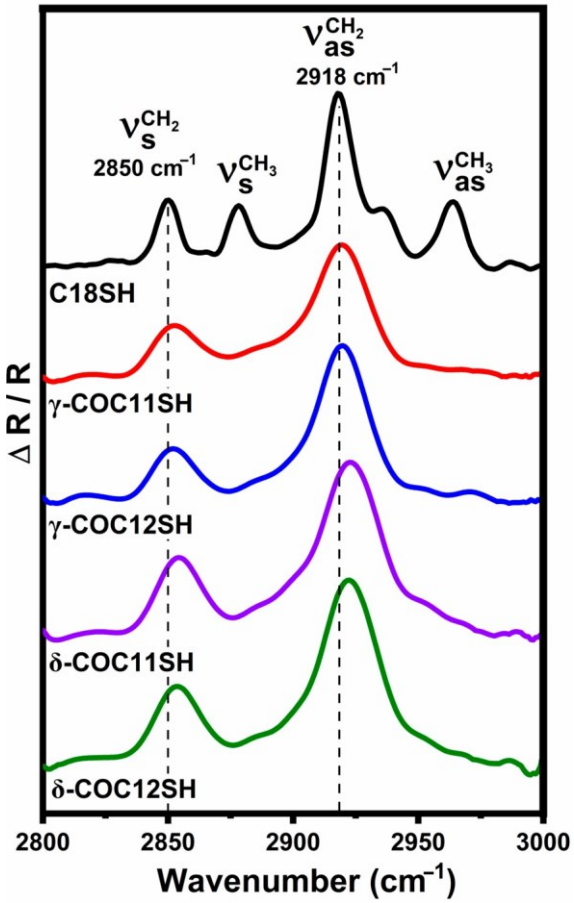

Figure 3. PM-IRRAS spectra of the C–H stretching region for SAMs derived from **C18SH**, **γ-COC11SH**, **γ-COC12SH**, **δ-COC11SH**, and **δ-COC12SH**.

Table 3. PM-IRRAS data for SAMs generated from C18SH, γ-COC11SH, γ-COC12SH, δ-COC11SH, and δ-COC12SH.

Adsorbate	$\nu_{s}^{CH_2}$ (cm^{-1})	$\nu_{s}^{CH_3}$ (cm^{-1})	$\nu_{as}^{CH_2}$ (cm^{-1})	$\nu_{as}^{CH_3}$ (cm^{-1})
C18SH	2850	2878	2918	2964
γ-COC11SH	2853	–	2920	–
γ-COC12SH	2853	–	2920	–
δ-COC11SH	2854	–	2923	–
δ-COC12SH	2854	–	2923	–

3.4. Wettability of the SAMs

The wetting properties of the lactone-terminated SAMs and their counterparts (PGA and PLGA) were investigated using a range of probe liquids. These liquids included polar protic solvents such as water (W), glycerol (Gly), formamide (FA), and *N*-methylformamide (MF); polar aprotic solvents such as dimethyl sulfoxide (DMSO), *N*,*N*-dimethylformamide (DMF), and acetonitrile (MeCN); and apolar aprotic solvents such as diiodomethane (DIM), decalin (DC), squalane (SQ), and hexadecane (HD). The surface tension values (γ_{LV}) of these probe liquids were reported as follows: water (γ_{LV} = 72.8 mN/m), glycerol (γ_{LV} = 64.0 mN/m), formamide (γ_{LV} = 58.2 mN/m), *N*-methylformamide (γ_{LV} = 38.0 mN/m), dimethyl sulfoxide (γ_{LV} = 43.7 mN/m), *N*,*N*-dimethylformamide (γ_{LV} = 37.1 mN/m), acetonitrile (γ_{LV} = 29.1 mN/m), diiodomethane (γ_{LV} = 50.8 mN/m), decalin (γ_{LV} = 31.5 mN/m), squalane (γ_{LV} = 28.9 mN/m), and hexadecane (γ_{LV} = 27.5 mN/m) [30,31].

Table 4 presents the advancing contact angles and hysteresis values (difference between advancing and receding contact angles) for various probe liquids on the surfaces of PGA

and PLGA, as well as the SAMs derived from **γ-COCnSH** and **δ-COCnSH**. The lactone-terminated SAM surfaces exhibited strong interactions and complete wetting with MF, DMSO, DMF, and MeCN, as did the PGA and PLGA surfaces. As expected, the probe liquids with low surface tensions (DC, SQ, and HD) also wet the surfaces [32–34].

Table 4. Advancing contact angles of the investigated SAMs and polymers using various probe liquids.

Adsorbate	Polar Protic Solvents				Polar Aprotic Solvents			Non-Polar Solvents			
	W	**Gly**	**FA**	**MF**	**DMSO**	**DMF**	**MeCN**	**DIM**	**DC**	**SQ**	**HD**
γ-COC11SH	55 (6)	50 (4)	37 (8)	<10 (–)	<10 (–)	<10 (–)	<10 (–)	26 (6)	<10 (–)	<10 (–)	<10 (–)
γ-COC12SH	57 (8)	54 (8)	38 (5)	<10 (–)	<10 (–)	<10 (–)	<10 (–)	28 (6)	<10 (–)	<10 (–)	<10 (–)
δ-COC11SH	72 (12)	64 (8)	52 (8)	<10 (–)	<10 (–)	<10 (–)	<10 (–)	33 (5)	<10 (–)	<10 (–)	<10 (–)
δ-COC12SH	77 (13)	68 (11)	59 (10)	<10 (–)	<10 (–)	<10 (–)	<10 (–)	37 (10)	<10 (–)	<10 (–)	<10 (–)
PGA	40 (9)	36 (6)	30 (7)	<10 (–)	<10 (–)	<10 (–)	<10 (–)	24 (4)	<10 (–)	<10 (–)	<10 (–)
PLGA	58 (12)	59 (6)	38 (12)	14 (–)	16 (5)	13 (–)	<10 (–)	33 (9)	<10 (–)	<10 (–)	<10 (–)

Values of hysteresis are given in parentheses. Water (W), glycerol (Gly), formamide (FA), *N*-methylformamide (MF), dimethyl sulfoxide (DMSO), *N*,*N*-dimethylformamide (DMF), acetonitrile (MeCN), diiodomethane (DIM), decalin (DC), squalane (SQ), hexadecane (HD).

Focusing on the probe liquids with measurable contact angles, Figure 4 illustrates the advancing contact angle values for water, formamide, glycerol, and diiodomethane on the studied surfaces. Notably, upon contact with water, the surfaces of PGA and PLGA exhibited noticeable swelling and potential reconstruction phenomena. To determine the contact angle of water, measurements were promptly taken within a 5 s interval following the initiation of contact. The contact angles of water were similar for the **γ-COC11SH** and **γ-COC12SH** SAMs (~55–57°), indicating comparable attractive interfacial interactions, likely arising from hydrogen bonding and/or dipole interactions [35,36]. In contrast, the **δ-COC11SH** and **δ-COC12SH** SAMs exhibited higher contact angles of water (~72–77°) compared to the **γ-COC11SH** and **γ-COC12SH** SAMs. This increased hydrophobicity can be attributed to the greater bulkiness of the six-membered lactone ring, which contains an additional methylene group, in the **δ-COC11SH** and **δ-COC12SH** SAMs, in contrast to the five-membered lactone ring in the **γ-COC11SH** and **γ-COC12SH** SAMs. The additional methylene group and increased bulkiness hinder hydrogen bonding and impede the polar interaction between the lactone groups and water molecules. The advancing contact angle values for glycerol, formamide, and diiodomethane were roughly similar on the **γ-COC11SH** and **γ-COC12SH** SAMs, while they were higher for the **δ-COC11SH** and **δ-COC12SH** SAMs. Comparing the wettabilities of the SAMs with those of the polymers, the wettabilities of PLGA towards the polar protic probe liquids (W, Gly, and FA) were more comparable to **γ-COCnSH** than to **δ-COCnSH**. Specifically, the wettability of **γ-COCnSH** towards the polar protic probe liquids exhibited a greater resemblance to that of PLGA compared to PGA. On the other hand, the wettabilities of PGA and PLGA towards the non-polar probe liquid (DIM) were more similar to **γ-COCnSH** and **δ-COCnSH**, respectively. This trend can be attributed to the presence of the bulkier lactone ring in **δ-COCnSH**, which leads to a higher contact angle with diiodomethane due to the larger steric bulk, in comparison to **γ-COCnSH**.

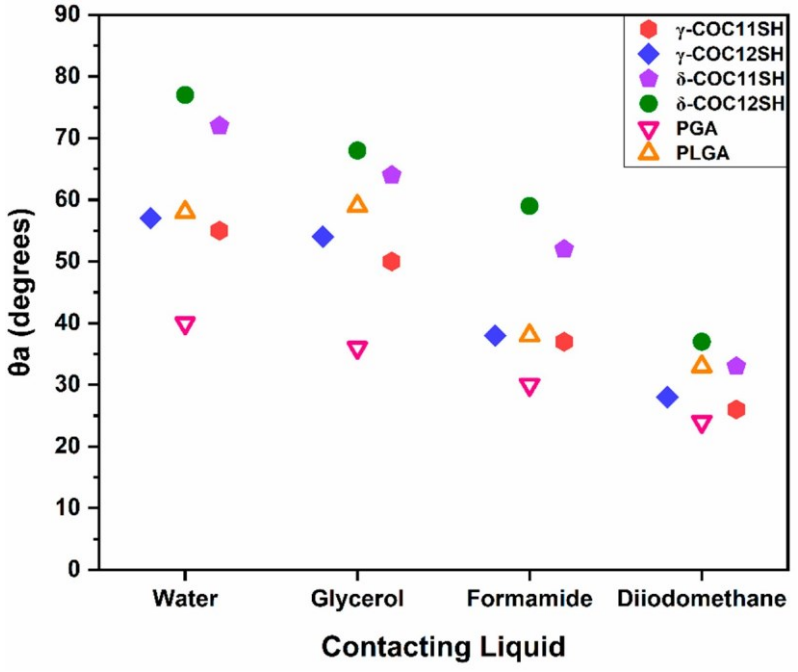

Figure 4. Advancing contact angle values measured on the lactone-terminated SAMs and the corresponding PGA and PLGA polymers. Error bars, which are not visible, fall within the symbols.

Interestingly, the contact angles of the polar protic probe liquids on the lactone SAMs and polymer surfaces, when ordered by surface tension (from highest to lowest), showed a decreasing trend as surface tension decreased. This trend can be explained by the decrease in surface tension, resulting from reduced intermolecular forces such as hydrogen bonding within the liquids, leading to stronger interactions with the surfaces and increased wettability. Moreover, the advancing contact angles exhibited by the polar protic liquids provide evidence that supports a model in which these liquids engage in favorable interfacial interactions (e.g., hydrogen bonding and/or dipole interactions) [35,36], with the lactone terminal groups present in the **γ-COCnSH** and **δ-COCnSH** SAMs. Likewise, the apolar aprotic liquids (decalin, squalene, and hexadecane), possessing lower surface tensions compared to diiodomethane, effectively wet the surfaces of both monolayers and polymers, owing to robust van der Waals interactions with the methylene groups present in the SAMs and polymers. Finally, the analysis of hysteresis data, which offers valuable information regarding surface roughness and potential heterogeneity such as surface reconstruction [37–39], demonstrated comparable values across all surfaces where reliable measurements of advancing and receding contact angles were obtained.

4. Conclusions

Two series of lactone-terminated thiol adsorbates, **γ-COCnSH** and **δ-COCnSH**, were designed, synthesized, and employed to generate nanoscale monolayers on gold substrates. The conformational characteristics of the resulting SAMs were analyzed using PM-IRRAS, specifically by examining the C–H antisymmetric stretching vibration of the alkyl spacer. The PM-IRRAS data revealed that the **γ-COCnSH** SAMs exhibited an all trans-extended conformation, whereas the **δ-COCnSH** SAMs displayed some gauche defects. To assess the packing densities of the monolayers, XPS measurements were performed to calculate integrated area of S/Au peaks. The results demonstrated that the **γ-COCnSH** SAMs exhibited higher packing densities and a more pronounced conformational order compared to the **δ-COCnSH** SAMs. Notably, contact angle measurements provided insights into the wettability of the surfaces. It was observed that the contact angle data for the **γ-COC11SH** and **γ-COC12SH** SAMs were remarkably similar to each other and to the contact angle values of the PLGA, rather than to PGA, surface across a broad range of probe liquids.

This suggests that the **γ-COCnSH** SAMs investigated in this study can effectively mimic nanoscale polyester surfaces, enabling the exploration of interfacial properties of polyesters in the absence of swelling and/or surface reconstruction phenomena.

Supplementary Materials: The following supporting information can be downloaded at https://www.mdpi.com/article/10.3390/chemistry6040039/s1, The Supplementary Materials include Schemes S1–S4: Details of the adsorbate synthesis; Figures S1–S8: Adsorbate characterization; Figures S9–S19: SAM characterization.

Author Contributions: Conceptualization, T.R.L.; methodology, P.T. and J.M.H.R.; validation, P.T., J.M.H.R., M.O. and J.M.L.; investigation, P.T., J.M.H.R., M.O. and J.M.L.; writing—original draft preparation, P.T. and H.-V.T.; writing—review and editing, T.R.L.; supervision, T.R.L. All authors have read and agreed to the published version of the manuscript.

Funding: The authors are grateful for generous financial support received from the National Science Foundation (CHE-2109174) and the Robert A. Welch Foundation (Grant No. E-1320).

Institutional Review Board Statement: Not applicable.

Informed Consent Statement: Not applicable.

Data Availability Statement: The data supporting this article have been included as part of the Supplementary Information.

Conflicts of Interest: There are no conflicts to declare.

References

1. Beckman, I.P.; Lozano, C.; Freeman, E.; Riveros, G. Fiber Selection for Reinforced Additive Manufacturing. *Polymers* **2021**, *13*, 2231. [CrossRef]
2. Jem, K.J.; Tan, B. The Development and Challenges of Poly(lactic acid) and Poly(glycolic acid). *Adv. Ind. Eng. Polym. Res.* **2020**, *3*, 60–70. [CrossRef]
3. Budak, K.; Sogut, O.; Aydemir Sezer, U. A Review on Synthesis and Biomedical Applications of Polyglycolic Acid. *J. Polym. Res.* **2020**, *27*, 208. [CrossRef]
4. Rocha, C.V.; Gonçalves, V.; da Silva, M.C.; Bañobre-López, M.; Gallo, J. PLGA-Based Composites for Various Biomedical Applications. *Int. J. Mol. Sci.* **2022**, *23*, 2034. [CrossRef]
5. Ong, C.S.; Lay, H.T.; Tamilselvam, N.R.; Chew, J.W. Cross-Linked Polycarbonate Microfiltration Membranes with Improved Solvent Resistance. *Langmuir* **2021**, *37*, 4025–4032. [CrossRef]
6. Ogieglo, W.; Ghanem, B.; Ma, X.; Pinnau, I.; Wessling, M. How Much Do Ultrathin Polymers with Intrinsic Microporosity Swell in Liquids? *J. Phys. Chem. B* **2016**, *120*, 10403–10410. [CrossRef]
7. Gugliuzza, A. Solvent Swollen Polymer. In *Encyclopedia of Membranes*; Drioli, E., Giorno, L., Eds.; Springer: Berlin/Heidelberg, Germany, 2016; pp. 1801–1802. [CrossRef]
8. Zaleski, R.; Krasucka, P.; Skrzypiec, K.; Goworek, J. Macro- and Nanoscopic Studies of Porous Polymer Swelling. *Macromolecules* **2017**, *50*, 5080–5089. [CrossRef]
9. Wang, J.; Klok, H.-A. Swelling-Induced Chain Stretching Enhances Hydrolytic Degrafting of Hydrophobic Polymer Brushes in Organic Media. *Angew. Chem. Int. Ed.* **2019**, *58*, 9989–9993. [CrossRef] [PubMed]
10. Tajalli, P.; Hernandez Rivera, J.M.; Omidiyan, M.; Tran, H.-V.; Lee, T.R. Carbonate-Terminated Self-Assembled Monolayers for Mimicking Nanoscale Polycarbonate Surfaces. *ACS Appl. Nano Mater.* **2023**, *6*, 2472–2477. [CrossRef]
11. Cooper, O.; Phan, H.-P.; Wang, B.; Lowe, S.; Day, C.J.; Nguyen, N.-T.; Tiralongo, J. Functional Microarray Platform with Self-Assembled Monolayers on 3C-Silicon Carbide. *Langmuir* **2020**, *36*, 13181–13192. [CrossRef]
12. Kahsar, K.R.; Schwartz, D.K.; Medlin, J.W. Control of Metal Catalyst Selectivity through Specific Noncovalent Molecular Interactions. *J. Am. Chem. Soc.* **2014**, *136*, 520–526. [CrossRef] [PubMed]
13. Coan, P.D.; Farberow, C.A.; Griffin, M.B.; Medlin, J.W. Organic Modifiers Promote Furfuryl Alcohol Ring Hydrogenation via Surface Hydrogen-Bonding Interactions. *ACS Catal.* **2021**, *11*, 3730–3739. [CrossRef]
14. Sui, W.; Zhao, W.; Zhang, X.; Peng, S.; Zeng, Z.; Xue, Q. Comparative Anti-Corrosion Properties of Alkylthiols SAMs and Mercapto Functional Silica Sol–Gel Coatings on Copper Surface in Sodium Chloride Solution. *J. Sol-Gel Sci. Technol.* **2016**, *80*, 567–578. [CrossRef]
15. Telegdi, J. Formation of Self-Assembled Anticorrosion Films on Different Metals. *Materials* **2020**, *13*, 5089. [CrossRef] [PubMed]
16. Choi, Y.; Tran, H.-V.; Lee, T.R. Self-Assembled Monolayer Coatings on Gold and Silica Surfaces for Antifouling Applications: A Review. *Coatings* **2022**, *12*, 1462. [CrossRef]
17. St. Hill, L.R.; Tran, H.-V.; Chinwangso, P.; Lee, H.J.; Marquez, M.D.; Craft, J.W.; Lee, T.R. Antifouling Studies of Unsymmetrical Oligo(Ethylene Glycol) Spiroalkanedithiol Self-Assembled Monolayers. *Micro* **2021**, *1*, 151–163. [CrossRef]

18. Barriet, D.; Chinwangso, P.; Lee, T.R. Can Cyclopropyl-Terminated Self-Assembled Monolayers on Gold Be Used to Mimic the Surface of Polyethylene? *ACS Appl. Mater. Interfaces* **2010**, *2*, 1254–1265. [CrossRef]
19. Yu, T.; Marquez, M.D.; Zenasni, O.; Lee, T.R. Mimicking Polymer Surfaces Using Cyclohexyl- and Perfluorocyclohexyl-Terminated Self-Assembled Monolayers. *ACS Appl. Nano Mater.* **2019**, *2*, 5809–5816. [CrossRef]
20. Rodriguez, D.; Marquez, M.D.; Zenasni, O.; Han, L.T.; Baldelli, S.; Lee, T.R. Surface Dipoles Induce Uniform Orientation in Contacting Polar Liquids. *Chem. Mater.* **2020**, *32*, 7832–7841. [CrossRef]
21. Bain, C.D.; Troughton, E.B.; Tao, Y.T.; Evall, J.; Whitesides, G.M.; Nuzzo, R.G. Formation of Monolayer Films by the Spontaneous Assembly of Organic Thiols from Solution onto Gold. *J. Am. Chem. Soc.* **1989**, *111*, 321–335. [CrossRef]
22. Choi, Y.; Park, C.S.; Tran, H.-V.; Li, C.-H.; Crudden, C.M.; Lee, T.R. Functionalized *N*-Heterocyclic Carbene Monolayers on Gold for Surface-Initiated Polymerizations. *ACS Appl. Mater. Interfaces* **2022**, *14*, 44969–44980. [CrossRef]
23. Zharnikov, M. High-Resolution X-ray Photoelectron Spectroscopy in Studies of Self-Assembled Organic Monolayers. *J. Electron Spectrosc. Relat. Phenom.* **2010**, *178–179*, 380–393. [CrossRef]
24. Chen, X.; Wang, X.; Fang, D. A Review on C 1s XPS-Spectra for Some Kinds of Carbon Materials. *Fuller. Nanotub. Carbon Nanostruct.* **2020**, *28*, 1048–1058. [CrossRef]
25. Aitchison, H.; Lu, H.; Hogan, S.W.L.; Früchtl, H.; Cebula, I.; Zharnikov, M.; Buck, M. Self-Assembled Monolayers of Oligophenylenecarboxylic Acids on Silver Formed at the Liquid–Solid Interface. *Langmuir* **2016**, *32*, 9397–9409. [CrossRef]
26. Ishida, T.; Hara, M.; Kojima, I.; Tsuneda, S.; Nishida, N.; Sasabe, H.; Knoll, W. High Resolution X-ray Photoelectron Spectroscopy Measurements of Octadecanethiol Self-Assembled Monolayers on Au(111). *Langmuir* **1998**, *14*, 2092–2096. [CrossRef]
27. Porter, M.D.; Bright, T.B.; Allara, D.L.; Chidsey, C.E.D. Spontaneously Organized Molecular Assemblies. 4. Structural Characterization of n-Alkyl Thiol Monolayers on Gold by Optical Ellipsometry, Infrared Spectroscopy, and Electrochemistry. *J. Am. Chem. Soc.* **1987**, *109*, 3559–3568. [CrossRef]
28. MacPhail, R.A.; Strauss, H.L.; Snyder, R.G.; Elliger, C.A. Carbon-Hydrogen Stretching Modes and the Structure of n-Alkyl Chains. 2. Long, All-Trans Chains. *J. Phys. Chem.* **1984**, *88*, 334–341. [CrossRef]
29. Snyder, R.G.; Strauss, H.L.; Elliger, C.A. Carbon-Hydrogen Stretching Modes and the Structure of n-Alkyl Chains. 1. Long, Disordered Chains. *J. Phys. Chem.* **1982**, *86*, 5145–5150. [CrossRef]
30. Smallwood, I. *Handbook of Organic Solvent Properties*; Butterworth-Heinemann: Woburn, MA, USA, 2014.
31. Wohlfarth, C. *Surface Tension of Pure Liquids and Binary Liquid Mixtures*, 2008th ed.; Lechner, M.D., Ed.; Landolt-Börnstein: Numerical Data and Functional Relationships in Science and Technology—New Series; Springer: Berlin/Heidelberg, Germany, 2008. [CrossRef]
32. Lee, S.; Park, J.-S.; Lee, T.R. The Wettability of Fluoropolymer Surfaces: Influence of Surface Dipoles. *Langmuir* **2008**, *24*, 4817–4826. [CrossRef]
33. Beitollahpoor, M.; Farzam, M.; Pesika, N.S. Determination of the Sliding Angle of Water Drops on Surfaces from Friction Force Measurements. *Langmuir* **2022**, *38*, 2132–2136. [CrossRef]
34. Beitollahpoor, M.; Farzam, M.; Pesika, N.S. Friction Force-Based Measurements for Simultaneous Determination of the Wetting Properties and Stability of Superhydrophobic Surfaces. *J. Colloid Interface Sci.* **2023**, *648*, 161–168. [CrossRef] [PubMed]
35. Soon Park, C.; Zenasni, O.; D Marquez, M.; Justin Moore, H.; Randall Lee, T. Hydrophilic Surfaces via the Self-Assembly of Nitrile-Terminated Alkanethiols on Gold. *AIMS Mater. Sci.* **2018**, *5*, 171–189. [CrossRef]
36. Lee, H.J.; Jamison, A.C.; Lee, T.R. Surface Dipoles: A Growing Body of Evidence Supports Their Impact and Importance. *Acc. Chem. Res.* **2015**, *48*, 3007–3015. [CrossRef]
37. Wang, J.; Wu, Y.; Cao, Y.; Li, G.; Liao, Y. Influence of Surface Roughness on Contact Angle Hysteresis and Spreading Work. *Colloid Polym. Sci.* **2020**, *298*, 1107–1112. [CrossRef]
38. Farzam, M.; Beitollahpoor, M.; Solomon, S.E.; Ashbaugh, H.S.; Pesika, N.S. Advances in the Fabrication and Characterization of Superhydrophobic Surfaces Inspired by the Lotus Leaf. *Biomimetics* **2022**, *7*, 196. [CrossRef]
39. Aktas, C.; Polat, O.; Beitollahpoor, M.; Farzam, M.; Pesika, N.S.; Sahiner, N. Force-Based Characterization of the Wetting Properties of LDPE Surfaces Treated with CF_4 and H_2 Plasmas. *Polymers* **2023**, *15*, 2132. [CrossRef]